Paleoceanography and Paleoclimatology

RESEARCH ARTICLE
10.1029/2017PA003221

Deepwater Expansion and Enhanced Remineralization in the Eastern Equatorial Pacific During the Last Glacial Maximum

N. E. Umling[1,2], R. C. Thunell[1], and M. Bizimis[1]

[1]School of the Earth, Ocean, and Environment, University of South Carolina, Columbia, SC, USA, [2]Department of Geology and Geophysics, Woods Hole Oceanographic Institution, Woods Hole, MA, USA

Key Points:
- The eastern equatorial Pacific experienced a shoaling of deep waters during the last glacial maximum
- A different mixture of deepwater masses bathed the eastern equatorial Pacific during the last glacial maximum
- Paired benthic foraminiferal Cd/Ca and carbon isotope measurements suggest increased remineralization in glacial middepth waters

Supporting Information:
- Supporting Information S1
- Data Set S1

Correspondence to:
N. E. Umling,
numling@whoi.edu

Citation:
Umling, N. E., Thunell, R. C., & Bizimis, M. (2018). Deepwater expansion and enhanced remineralization in the eastern equatorial Pacific during the last glacial maximum. *Paleoceanography and Paleoclimatology*, *33*, 563–578. https://doi.org/10.1029/2017PA003221

Received 24 JUL 2017
Accepted 2 MAY 2018
Accepted article online 15 MAY 2018
Published online 4 JUN 2018

Abstract Published estimates of the radiocarbon content of middepth waters suggest a decrease in ventilation in multiple locations during the last glacial maximum (LGM; 24.0–18.1 ka). Reduced glacial ventilation would have allowed respired carbon to accumulate in those waters. A subsequent deglacial release of this respired carbon reservoir to the atmosphere could then account for the observed increases in atmospheric CO_2 and decline in atmospheric radiocarbon content. However, age model error and a release of ^{14}C-depleted mantle carbon have also been cited as possible explanations for the observed middepth radiocarbon depletions, calling into question the deep ocean's role in storing respired carbon during the LGM. Joint measurements of benthic foraminiferal carbon isotope values ($\delta^{13}C$) and cadmium/calcium (Cd/Ca) ratios provide a method for isolating the air-sea component of a water mass from changes in remineralization. Here we use benthic foraminiferal $\delta^{13}C$ and Cd/Ca records from the eastern equatorial Pacific to constrain changes in remineralization and water-mass mixing over the last glacial-interglacial transition. These records are complemented with elemental measurements of the authigenic coatings of foraminifera to monitor postdepositional changes in bottom water properties. Our results suggest an increase of deep waters at midwater depths consistent with a shoaling of the boundary between the upper and lower branches of Southern Ocean overturning circulation. Additionally, our records demonstrate increased organic matter remineralization in middepth waters during the LGM, suggesting that respired carbon did accumulate in middepth waters under periods of reduced ventilation.

Plain Language Summary Records of gas bubbles trapped in ice suggest that the concentration of CO2 in the atmosphere was lower during cold, glacial periods when ice covered more of Earth. These records show that both atmospheric CO2 and temperature increased as Earth's climate transitioned from last glacial period, about 20,000 years ago, to the warmer climate Earth has experienced over the last 10,000 years. Data suggest that the oceans are a significant source of this CO2. During ocean circulation, a water mass sinks from the surface of the ocean where it is no longer exchanging CO2 with the atmosphere, allowing the CO2 to accumulate in those waters. To investigate whether the oceans stored CO2 during the last glacial period, we developed records of past ocean chemistry using the shells of small marine organisms that record the chemistry of the water they are living in as they build their shells. Our results from the eastern equatorial Pacific indicate that CO2 accumulated in these waters during the last glacial, likely as a result of changes in ocean circulation. By understanding how the oceans and atmosphere have exchanged CO2 in the past, we better understand what role the oceans may play under modern CO2 increases.

1. Introduction

Changes in atmospheric CO_2 are thought to amplify insolation variability associated with the orbital cycles, driving the transition between glacial and interglacial climate states over at least the last ~800 kyr (Galbraith & Eggleston, 2017; Sigman & Boyle, 2000). The abrupt CO_2 increases during the last deglaciation (Marcott et al., 2014) provide an opportunity to study the relationship between increasing CO_2 and rapid warming of atmospheric temperatures. Because of the size and mobility of the deep ocean carbon reservoir, it has been implicated as the primary source of CO_2 to the atmosphere during deglaciation (Broecker, 1982; Broecker & Barker, 2007). Furthermore, Antarctic ice cores record decreasing atmospheric radiocarbon values simultaneous with increasing CO_2 (Hughen et al., 2000; Marcott et al., 2014; Monnin et al., 2001; Sikes et al., 2016; Skinner et al., 2015), indicating that the CO_2 source to the atmosphere came from a ^{14}C-depleted reservoir.

It has been hypothesized that changes in Southern Ocean meridional overturning circulation driven by increased sea ice extent or stratification allowed respired carbon to accumulate in the deep ocean during the LGM (Anderson et al., 2009; Keeling & Stephens, 2001; Toggweiler et al., 2006; Watson et al., 2015). Isolation of deep waters would have allowed ^{14}C to decay, thus providing a source for the ^{14}C-depleted carbon delivered to the atmosphere during deglaciation (Broecker & Barker, 2007; Hughen, 2004; Hughen et al., 1998). Additionally, changes in the efficiency of the oceanic biological pump have been linked to the glacial-interglacial transfer of CO_2 between the oceans and atmosphere (Bauska et al., 2016; Hertzberg et al., 2016; Jaccard et al., 2016; Pichevin et al., 2009; Ziegler et al., 2013). However, it has been estimated that the biological pump could only have contributed up to half of the observed CO_2 flux (Kohfeld, 2005), necessitating an additional process such as ventilation to achieve the full glacial-interglacial CO_2 change.

Recent evidence suggests that respired carbon primarily accumulated in middepth waters rather than deep waters during the LGM (Burke et al., 2015; Cook & Keigwin, 2015; Lund, 2013; Ronge et al., 2016; Sikes et al., 2000, 2016; Skinner et al., 2015) due to shoaling of the isopycnal separating the upper and lower branches of Southern Ocean overturning circulation (SOOC; Burke et al., 2015; Ferrari et al., 2014; Ronge et al., 2016; Skinner et al., 2010). As this isopycnal shoals above ~2 km water depth, it interacts with fewer bathymetric features resulting in decreased turbulent mixing between the upper and lower branches of SOOC (Ferrari et al., 2014). This would have allowed radiocarbon to decay and respired carbon to accumulate in middepth waters during the LGM. Alternatively, it has been proposed that the low ^{14}C values documented in cores located close to oceanic spreading centers may have been influenced by an increase in mantle-derived ^{14}C-depleted carbon (Hasenclever et al., 2017; Lund et al., 2016; Ronge et al., 2016). It is not known whether the low ^{14}C values were indeed influenced by increased input of mantle-derived ^{14}C-depleted carbon or whether a shoaling of the upper and lower branches of SOOC allowed respired carbon to accumulate in middepth waters of the eastern equatorial Pacific (EEP; de la Fuente et al., 2015; Hasenclever et al., 2017; Lund et al., 2016; Umling & Thunell, 2017).

Here we characterize the water masses of mid (1.0–3.0 km) and deep waters (>3.0 km) of the eastern equatorial Pacific during the last 25,000 years utilizing coupled measurements of benthic foraminiferal $\delta^{13}C$ Cd/Ca from a transect of sediment cores from the Panama Basin. Cadmium is tightly coupled with the nutrient phosphate in the world's oceans, and foraminiferal Cd/Ca ratios have been shown to record the seawater cadmium concentrations with a depth-dependent fractionation (Boyle, 1992). Similarly, the distribution of $\delta^{13}C$ is related in part to the preferential fractionation of ^{12}C during photosynthesis (Broecker & Peng, 1982), resulting in elevated $\delta^{13}C$ in marine surface waters and depleted $\delta^{13}C$ in deeper waters. As surface waters equilibrate with the atmosphere during air-sea gas exchange, there is an additional isotopic fractionation of carbon during CO_2 exchange with the atmosphere (Inoue & Sugimura, 1985). This fractionation is temperature dependent, with a larger fractionation of $\delta^{13}C$ in cold, high latitudes relative to warmer, low latitudes (Broecker & Peng, 1982; Charles et al., 1993; Lynch-Stieglitz et al., 1995). Therefore, the $\delta^{13}C$ value of a water mass reflects fractionation related to air-sea exchange, temperature, surface water residence times, and photosynthesis (Broecker & Peng, 1982; Charles et al., 1993; Lynch-Stieglitz et al., 1995). By utilizing Cd/Ca to constrain the nutrient concentration, the biological ($\delta^{13}C_{bio}$) and physical components ($\delta^{13}C_{as}$) of $\delta^{13}C$ can be isolated from the measured $\delta^{13}C$ (Lynch-Stieglitz et al., 1995; Lynch-Stieglitz & Fairbanks, 1994). Together, measurements of benthic foraminiferal Cd/Ca and $\delta^{13}C$ provide information on both water mass source and deepwater mixing, along with nutrient utilization.

2. Sample Material and Oceanographic Setting

This study utilizes a series of cores collected from intermediate and deep water depths (1,620–3,200 m) of the Panama Basin during R/V Trident cruise TR-163 (Table 1 and Figure 1). The Panama Basin is a semienclosed basin bounded by South and Central America to the north and east. The Carnegie and Cocos submarine ridges form the southern and northwest boundaries of the basin, converging westward toward the volcanically active Galapagos Islands. The Galapagos spreading center extends eastward along 1°N toward the center of the basin and northeast from the center of the basin toward Panama. These features are potential sources of volcanic and hydrothermal products to the basin (Pedersen, 1979). Deepwater cores TR163-23 and TR163-20B were collected off the west flank of the Galapagos platform at depths of 2,730 and

Table 1
Eastern and Western Equatorial Pacific Core Locations, Depths, and References

Core	Latitude	Longitude	Core depth	Sedimentation rate (cm/kyr)	Reference
Eastern equatorial Pacific cores					
V19-27	0.47	−82.07	1373	5	Boyle (1992)
TR163-2	8.24	−84.35	1620	2.1	This study
V17-42	3.53	−81.18	1841	5.8	Boyle (1992)
TR163-18	2.81	−89.85	2030	2.1	This study
TR163-14	3.91	−87.24	2365	4.7	This study
TR163-25	−1.65	−88.45	2650	6.5	This study
V19-28	−2.37	−84.85	2720	4.4	Boyle (1992)
TR163-23	0.41	−92.16	2730	9.4	This study
V19-30	−3.38	−82.35	3071	9	Boyle (1988, 1992)
TR163-20B	0.79	−93.84	3200	10.1	This study
TR163-31B	−3.62	−83.97	3210	7.7	Boyle (1988)
RC10-65	−0.68	−108.62	3588	6.7	Boyle (1988)
KNR73-3	0.37	−106.18	3606	<2	Boyle (1988, 1992)
KNR73-4	10.85	−110.27	3681	<2	Boyle (1988, 1992)
Western equatorial Pacific cores					
V32-159	48.67	147.4	1235		Boyle (1992)
V32-161	48.28	149.07	1600	7.6	Boyle (1992)
V28-235	−5.45	160.48	1748	1.3	Boyle (1992)
V24-109	0.43	158.8	2367	3.4	Boyle (1988)
V26-304	28.53	134.13	2942		Boyle (1992)
Rama 44	53.01	164.65	2980	9.2	Boyle (1992)
V28-238	1.02	160.48	3120	1.8	Boyle (1992)
V32-128a	36.47	177.17	3623	2.7	Boyle (1992)
V32-126	35.32	174.9	3870		Boyle (1992)

Note. Sedimentation rates are not included for cores with only core-top data available.

3,200 m, respectively. TR163-25 was collected from the Carnegie Ridge, and the three shallowest cores were collected from the Cocos Ridge (Figure 1).

The age model for TR163-23 was constructed using calibrated radiocarbon ages with a variable reservoir age as previously reported (Umling & Thunell, 2017). The age models for the other TR163 cores were developed by tuning *Globigerinoides ruber* $\delta^{18}O$ from each of the cores to the *G. ruber* $\delta^{18}O$ of TR163-23 (Figure 2). The age of the LGM was constrained for each of the low accumulation rate cores (2–4 cm/kyr) TR163-2, TR163-14, and TR163-18. The higher accumulation rate (>6 cm/kyr) cores TR163-25 and TR163-20B included additional $\delta^{18}O$ tie-points during the deglaciation (Figure 2). A *Neogloboquadrina dutertrei* ^{14}C age ($\Delta R = 147 \pm 13$) was used to constrain the Holocene for each of the TR163 cores. The Elastic Tie-Pointing method of Heaton et al. (2013) was used to transfer tie-point ages from TR163-23 to corresponding depths in cores TR163-25 and TR163-20B. Final age models were constructed using the Bayesian age-depth modeling program Bacon from Blaauw and Christen (2011). No distinct ash layers were found in any of the cores, but TR163-23 occasionally contained dispersed volcanic debris mainly composed of amber-brown to clear volcanic shards. These glass shards are consistent with microtephra described from nearby core TR163-22 (Lea et al., 2005), and similar deposits have been described for the Panama Basin by Kowsmann (1973) and attributed to subaerial eruptions or extremely shallow submarine vents.

The EEP is a region characterized by a shallow thermocline and the upwelling of nutrient-rich waters. In particular, surface waters near the Galapagos Islands are highly productive due to upwelling of the Equatorial Undercurrent (Pennington et al., 2006). The basin is also marked by a strong meridional sea surface temperature (SST) gradient. The southern part of the basin is located within the equatorial cold-tongue with SST increasing northward across the basin into the eastern Pacific warm-pool (Fiedler & Talley, 2006). The world's largest oxygen minimum zones are located in the eastern Pacific, north and south of the equator at depths of ~250–1,000 m (Kamykowski & Zentara, 1990). At present, abyssal waters (>3,500 m) in the EEP originate from Lower Circumpolar Deep Waters that have been modified by geothermal heating within deep basins of the eastern Pacific (Lonsdale, 1976; Tsuchiya & Talley, 1998). These waters are overlain by Pacific Deep Water

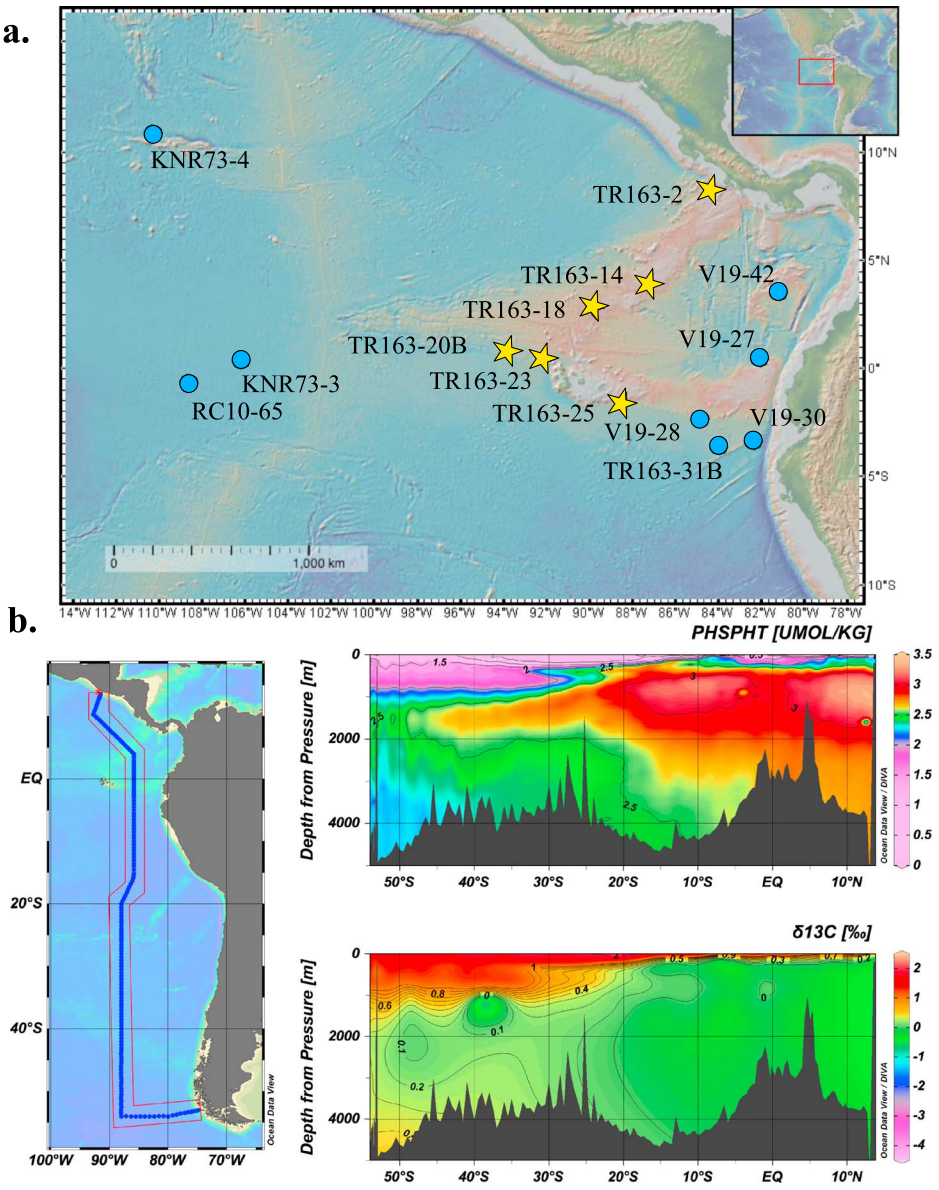

Figure 1. (a) The location of eastern equatorial Pacific benthic foraminiferal Cd_W records from this study (stars) and Boyle (1988, 1992, circles). (b) Phosphate and $\delta^{13}C$ from the P19 GLODAP section (Key et al., 2004) provide modern end-member values. Phosphate and cadmium are closely linked in the modern ocean, with a phosphate maximum occurring at ~1.0 km in the Pacific. Equatorial Pacific deep waters fall along a mixing line between the North Pacific $\delta^{13}C$ end-member (~ −0.4‰) and Southern Ocean end-member (~0.5‰; Key et al., 2004). Figure developed using the Ocean Data View software of Schlitzer (2015).

(PDW) at middepths (~1,000–3,200 m) and by Equatorial Pacific Intermediate Water (EqPIW) at shallower depths (~700–1000 m; Tsuchiya & Talley, 1998). Mixing between North Pacific Intermediate Water (NPIW), Antarctic Intermediate Water (AAIW), and upwelled PDW is responsible for the composition of EqPIW (Bostock et al., 2010).

The heterogeneous distribution of hydrothermal and volcanic activity, along with variable surface productivity and water-column oxygenation, sets up a complex geochemical environment within the Panama Basin. Precipitation of manganese-carbonate phases have been documented (Boyle, 1983; Pedersen & Price,

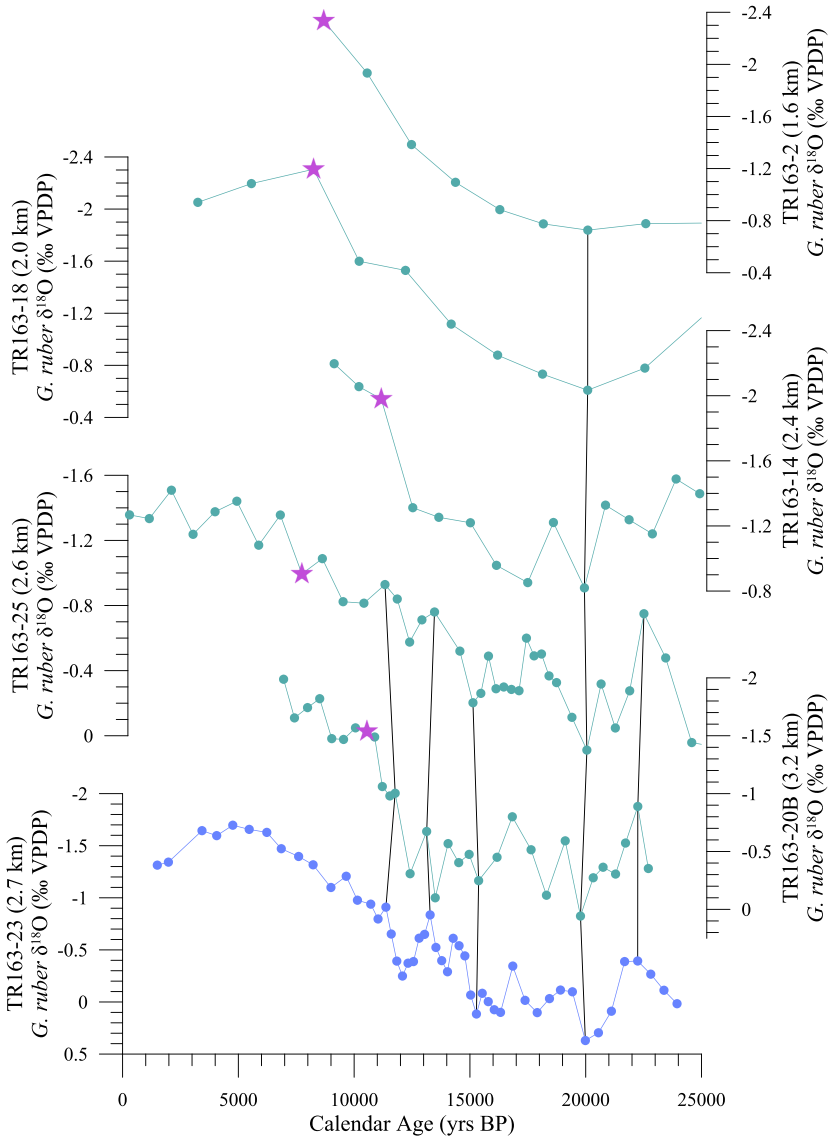

Figure 2. *Globigerinoides ruber* $\delta^{18}O$ was used to link TR163 cores to the age model of TR163-23 from Umling and Thunell (2017). The purple stars indicate samples used for Holocene radiocarbon age constraint, and the black lines connect tie-points between TR163-23 and other TR163 cores. In low accumulation rate cores TR163-2, TR163-18, and TR163-14, a single tie-point for the LGM was identified as the point of maximum $\delta^{18}O$ values.

1982; Pena et al., 2008) in Panama Basin sediments along with Al-silicate contamination (Lea et al., 2005). These conditions require careful cleaning of foraminiferal samples along with close monitoring of authigenic and biogenic element compositions.

3. Methods

Carbon isotopes were measured on specimens of the benthic foraminifera *Cibicidoides wuellerstorfi* from three TR163 cores with sedimentation rates >5 cm/kyr (TR163-20B, TR163-23, and TR163-25). All analyses were carried out on a GV Isoprime stable isotope ratio mass spectrometer. The long-term reproducibility of $\delta^{13}C$ measurements is 0.06‰, and all samples are reported relative to the Vienna Peedee belemnite scale. Samples for isotopic analysis were cleaned in 3% H_2O_2 to remove organic material and then briefly sonicated in acetone to remove adhered particles. *Cibicidoides wuellerstorfi* is ideal for monitoring past deep-ocean chemistry as it has an epifaunal habitat and has been shown to incorporate carbon isotopes in a roughly 1:1 ratio with bottom water (Mackensen, 2008; Schmittner et al., 2017).

Samples of 5–15 *C. wuellerstorfi* were cleaned for trace element analysis following the Cd-cleaning protocol from Boyle and Keigwin (1985) as modified by Boyle and Rosenthal (1996) using the minimal settling technique from Barker et al. (2003). All analyses were carried out on a Thermo Element II high-resolution inductively coupled plasma–mass spectrometry at the Center for Elemental Mass Spectrometry at the University of South Carolina. To minimize matrix effects, the Ca content of each analyzed sample solution was matched to a gravimetrically made standard at 20 ppm Ca, by first performing a dip check and diluting the sample. The analytical reproducibility for Cd/Ca is ±0.003 μmol/mol (± 3.7%) based on repeated measurements of a standard of ~0.190 μmol/mol.

We monitored Al-silicate and oxide contamination through concurrent analysis of diagenetic indicators Fe/Ca, Mn/Ca, and Al/Ca. The Fe/Ca values were generally low (<50 mmol/mol) in all TR163 cores; samples with elevated Fe/Ca values (>100 mmol/mol) were excluded. In contrast, Mn/Ca and Al/Ca values were commonly elevated (>100 μmol/mol) with increasing Mn/Ca values with depth and higher Al/Ca values generally found in the middepth cores. High Al/Ca and Mn/Ca values are not unusual for Panama Basin sediment cores, with precipitation of Mn-carbonate coatings (Boyle, 1983; Pena et al., 2005, 2008), formation of Mn-oxides (Balistrieri & Murray, 1986), hydrothermal activity (Klinkhammer et al., 1977; Marchig et al., 1984), and volcanic debris (Lea et al., 2005) all serving as sources of Mn in this region. Because of the high spatial variability and differing chemical impacts of these processes, it has been proposed that identification of acceptable trace element data should utilize site-specific contamination thresholds (Lea et al., 2005). Here samples with anomalous Al/Ca and Mn/Ca values (>500 μmol/mol) were excluded from data analyses; however, a higher threshold was required for TR163-20B Mn/Ca values (>1,000 μmol/mol) as the mean Mn/Ca value for this core was ~520 μmol/mol. Low Fe/Ca values for TR163-20B suggest that the high foraminiferal Mn/Ca for this core is not associated with Fe oxides. Furthermore, Mg/Ca values from this core are not anomalously high as is the case with contamination from manganese-carbonate overgrowths (Boyle, 1983; Pena et al., 2005, 2008). Sedimentary enrichments of Mn have been attributed to flux from a high-Mn hydrothermal plume (Klinkhammer et al., 1977; Pedersen, 1979) and could be responsible for the elevated Mn/Ca in this core. Despite the higher threshold of Mn/Ca for TR163-20B, the Cd/Ca results from this core agree with previously reported Cd/Ca values from a similar depth Panama Basin core (TR163-31B; Boyle, 1988). Furthermore, the cleaned benthic Cd/Ca values for TR163-20B are not significantly correlated with Mn/Ca, Fe/Ca, or Al/Ca values (Figure S1).

The cadmium concentration of seawater was estimated from the cleaned benthic foraminiferal Cd/Ca values using the empirical depth-dependent Cd distribution coefficient (D) of Boyle (1992) and normalizing Cd values for the average concentration of cadmium in seawater (0.01 mol/kg). For water depths greater than 3.0 km, D = 2.9, and for water depths 1.15–3.0 km, the equation from Boyle (1992) was used (equation (1)).

$$D = 1.3 + (\text{depth}–1150)^{*}\ (1.6/1850) \tag{1}$$

The air-sea signature of $\delta^{13}C$ ($\delta^{13}C_{as}$) was estimated using the Holocene (equation (2)) and glacial (equation (3)) equations of Lynch-Stieglitz and Fairbanks (1994) for $PO_3^{-4} > 1.3$ μmol/kg.

$$\delta^{13}C_{as} = \delta^{13}C_{\text{measured}} + 2.75^{*}Cd_W–2.0 \tag{2}$$

$$\delta^{13}C_{as} = \delta^{13}C_{\text{measured}} + 2.375^{*}Cd_W–1.46 \tag{3}$$

Major (^{43}Ca), minor (^{55}Mn), trace (^{27}Al, ^{47}Ti, ^{51}V, ^{53}Cr, ^{57}Fe, ^{59}Co, ^{60}Ni, ^{63}Cu, ^{111}Cd, and ^{238}U), and rare earth (^{89}Y, ^{139}La, ^{140}Ce, ^{141}Pr, ^{145}Nd, ^{146}Nd, ^{147}Sm, ^{151}Eu, ^{157}Gd, ^{159}Tb, ^{163}Dy, ^{165}Ho, ^{167}Er, ^{169}Tm, ^{173}Yb, and ^{175}Lu) element concentrations were measured on 50 mg samples of mixed planktonic foraminifera from the >355 μg size fraction using a Thermo Element II high-resolution inductively coupled plasma–mass spectrometry. Foraminifera were gently crushed to open shell chambers and cleaned for adhering clays using repeated ultrasonication and rinses of water and methanol (Boyle, 1981). Any remaining visible coarse-grained silicates were removed by cleaning using a fine brush under a binocular microscope (Barker et al., 2003). A spike solution artificially enriched in ^{145}Nd was added to measured samples and blanks as internal standard. Briefly, the ^{145}Nd/^{146}Nd was used to calculate the absolute Nd concentration of each sample by isotope dilution, following the method of Willbold et al. (2003). The Nd concentration and the spike-corrected ^{146}Nd-signal then became the internal standard to monitor drift and quantify concentrations using ^{146}Nd-normalized signals. We used the USGS reference material BHVO-2 as an external standard for

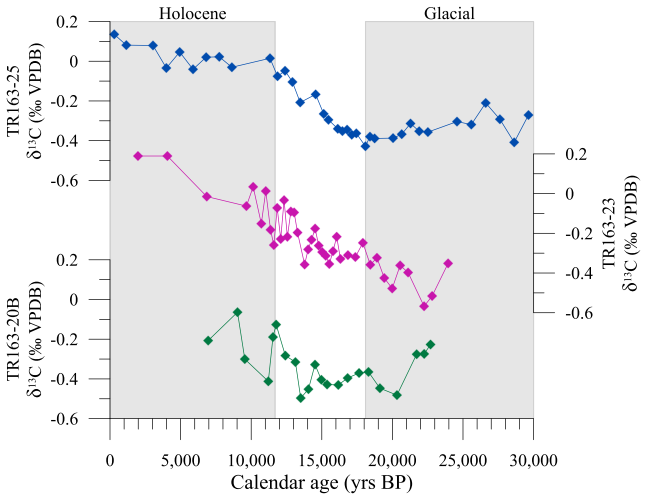

Figure 3. Benthic foraminiferal carbon isotopic composition of *C. wuellerstorfi* for cores TR163-25 (2.65 km), TR163-23 (2.73 km), and TR163-20B (3.20 km).

quantification of the samples. The Nd-concentrations are reproducible to within 1%. Overall precision and accuracy of the method are better than 5% for all elements. Full procedural blanks were corrected for and are insignificant (<1%) for all reported elements. Rare earth element (REE) concentrations were normalized to Post-Archaean Australian Shale (Taylor & McLennan, 1985).

4. Results

The *C. wuellerstorfi* $\delta^{13}C$ values for TR163-25 and TR163-23 increase over the last glacial-interglacial transition by ~0.5‰ (Figure 3). This is consistent with the documented mean whole ocean glacial-interglacial $\delta^{13}C$ increase of ~0.46‰ (Curry et al., 1988). The Holocene average $\delta^{13}C$ values of 0.04‰ and −0.03‰ for TR163-25 and TR163-23, respectively, are within error (±0.06‰) of the modern EEP $\delta^{13}C$ value recorded for middepth waters (~0‰; Key et al., 2004). The $\delta^{13}C$ values for TR163-20B generally increase from the last glacial to the early Holocene by ~0.3‰ but record a brief return to glacial $\delta^{13}C$ values during the early Holocene (Figure 3). The eastern equatorial Pacific cores document a glacial-Holocene difference in the seawater cadmium concentration (Cd_W) of ~0.2 nmol/kg at 2.73 km water depth (TR163-23), with values increasing from ~0.7 nmol/kg during the LGM to ~0.9 nmol/kg in the Holocene (Figure 4). Slightly larger glacial-interglacial Cd_W increases are recorded at shallower depths: 0.3 nmol/kg at 1.62 and 2.03 km water depth (TR163-2 and TR163-18, respectively) and 0.4 nmol/kg at 2.65 km water depth (TR163-25; Figure 4). Holocene Cd_W averages for the cores used in this study are similar to eastern and western equatorial Pacific Cd_W values determined from the core-top benthic foraminiferal Cd/Ca data (Boyle, 1988, 1992; Table 1 and Figure 5). As with EEP present-day water column measurements (Key et al., 2004), our EEP foraminiferal Cd_W decreases slightly from 1.0 to 4.5 km water depth during both the Holocene and LGM (Figure 5). However, during the Holocene, EEP foraminiferal mean Cd_W values are slightly higher (~0.2 nmol/kg) in middepth waters relative to present-day water column values. This middepth feature was enhanced during the LGM, with EEP mean Cd_W values being up to ~0.6 nmol/kg higher at ~2.0 km water depth, relative to the WEP (Figure 5). Additionally, the variability of foraminiferal Cd_W also increases during the LGM at these depths.

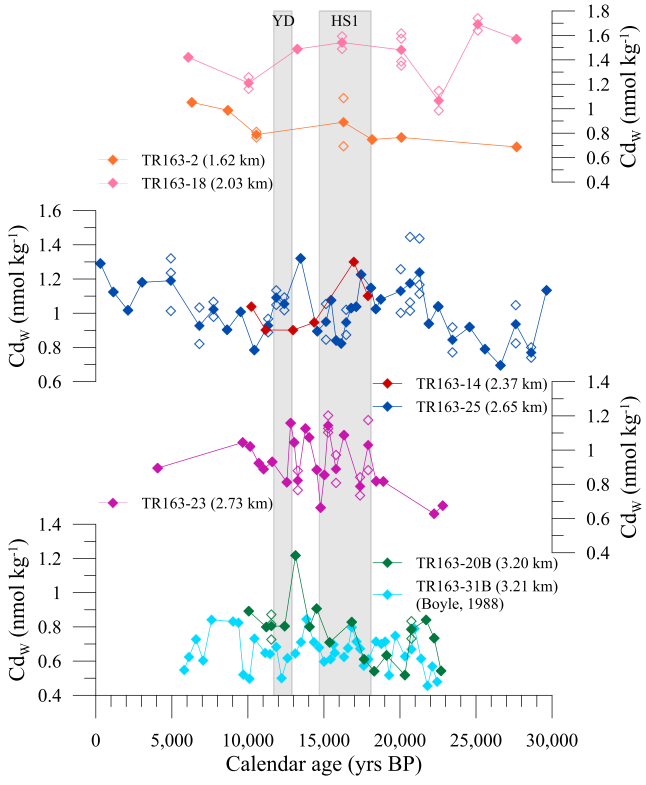

Figure 4. Seawater cadmium (Cd_W) has been estimated for TR163 cores from the Cd/Ca values of *C. wuellerstorfi* and *C. mundulus* (only TR163-2). A new age model for TR163-31B was estimated using the Bayesian age-depth modeling program BACON (Blaauw & Christen, 2011) to calibrate the *N. dutertrei* radiocarbon ages of Shackleton et al. (1988) utilizing variable reservoir ages reported in Umling and Thunell (2017).

To assess possible geochemical influences on the foraminiferal Cd/Ca, authigenic REE and trace element compositions were measured on selected bulk planktonic foraminifera samples from deepwater core TR163-20B and middepth core TR163-14. The concentration of certain metals (Ni, Co, Cd, Ba, and Zn) in marine sediments has been shown to increase with the formation of Mn-oxides (Balistrieri & Murray, 1986; Tribovillard et al., 2006). Pearson's correlation coefficients indicate that Mn has strong ($r^2 > 0.8$) correlations with Cd and Co and a moderately strong correlation ($0.6 < r^2 < 0.8$) with Ni in TR163-14 (Table 2). However, these elements were only mildly ($r^2 < 0.4$) correlated with Mn in deepwater core, TR163-20B. Element characteristic of reducing environments (U, V, and Cr; Tribovillard et al., 2006) showed only mild to modest correlations with Mn from TR163-14 (Table 2). The average concentration of authigenic Mn is enriched in TR16-20B (~400 ppm) relative to TR163-14 (~75 ppm), but the reverse is true for the average authigenic Cd concentration of TR163-20B (~0.08 ppm) relative to TR163-14 (~0.42 ppm).

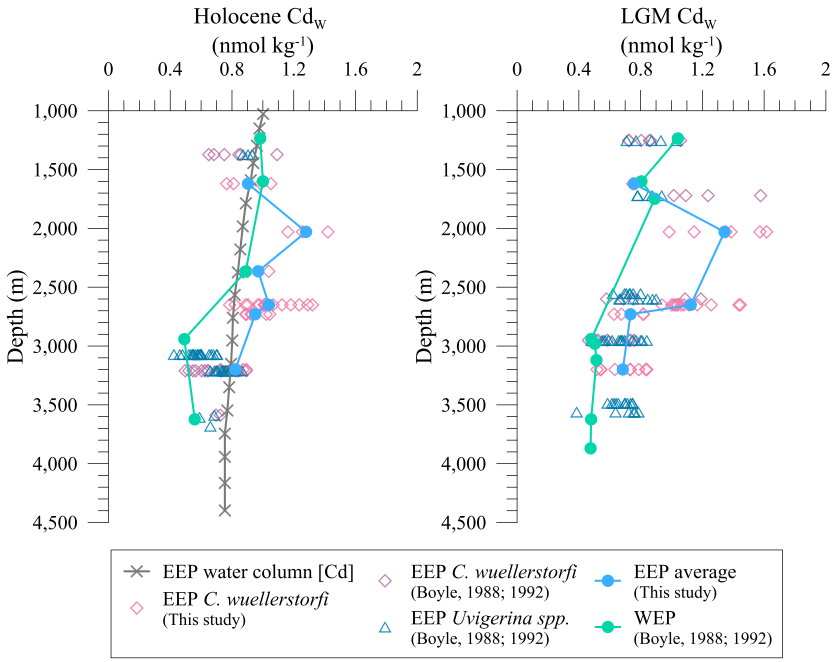

Figure 5. Average eastern equatorial Pacific Holocene and LGM Cd_W were estimated for a transect of cores from 1.37–3.68 km water depth using the Cd/Ca data of this study and Boyle (1988, 1992). Eastern equatorial Pacific water column Cd was estimated from GLODAP station 1894 phosphate (Key et al., 2004) using the relationship Cd(nmol/kg) = 0.4*P(μmol/kg) − 0.25 from Boyle (1988). Water depths for the LGM have been adjusted by 120 m to account for lower sea levels.

Rare earth element profiles from both TR163-14 and TR163-20B record depletions in cerium relative to neighboring REEs (La and Nd; Figure 6). For consistency with previous studies the cerium anomaly (Ce/Ce*) was calculated here using the equation from German and Elderfield (1990; equation (4)).

$$Ce/Ce^{*} = 3{\cdot}Ce/(2{\cdot}La + Nd) \quad (4)$$

Negative cerium anomalies (Ce/Ce* < 1) are a common feature in seawater and occur due to the oxidation of Ce(III) to Ce(IV) in the water column followed by rapid scavenging onto particles (Elderfield & Greaves, 1982). This results in a positive correlation of Ce/Ce* with water-mass age (German & Elderfield, 1990). However, this signal can be overprinted by the pore water reduction of Ce(IV) to Ce(III) under suboxic conditions resulting in a negligible (Ce/Ce* = 1) or positive (Ce/Ce* > 1) cerium anomaly (Wright et al., 1987). TR163-20B and TR163-14 are marked by negative cerium anomalies throughout (Figure 7). TR163-20B records relatively constant Ce/Ce* values of ~0.3 for EEP deep waters from the LGM through the early Holocene (Figure 7). In contrast, middepth core TR163-14 records Ce/Ce* values of ~0.6 during the LGM with an abrupt decrease at ~13.0 ka to values of ~ 0.4 during the early Holocene. The cerium anomaly shows a strong negative correlation with Mn for middepth core TR163-14 whereas Ce/Ce* and Mn are only mildly correlated for deepwater core TR163-20B (Table 2).

Table 2
Pearson Correlation Coefficients of Bulk Planktonic Authigenic Mn and Cd

	Li	Al	Ca	Ti	V	Cr	Mn	Fe	Co	Ni	Cu	U	Ce/Ce*
Cd	−0.19	−0.03	0.45	−0.16	0.39	−0.57	**0.94****	0.43	**0.96****	**0.93****	−0.11	−0.39	**−0.82***
	0.5	−0.53	**0.84***	−0.49	0.56	−0.28	0.5	−0.5	**0.64**	**0.95****	−0.25	**0.9** *	−0.14
Mn	−0.32	0.04	0.46	−0.11	0.42	**−0.67**		0.55	**0.9** **	**0.88** *	0.31	0.52	**−0.92** **
	0.97**	−0.58	**0.74**	−0.14	0.12	**−0.8***		−0.35	0.19	**0.61**	−0.39	**0.62**	**−0.65**

Note. The bold font indicates a moderately strong correlation (>0.6), and the filled background indicates a strong correlation (>0.8). Correlation coefficients for TR163-14 are indicated in blue and in red for TR163-20B.
*Statistically significant ($p < 0.05$). **Highly statistically significant ($p < 0.001$).

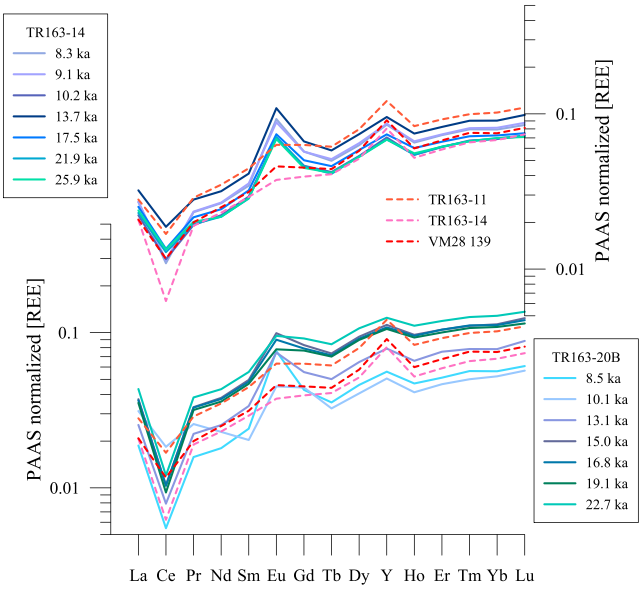

Figure 6. The PAAS-normalized distribution of rare earth elements at 2.37 km (TR163-14) and 3.2 km (TR163-20B) compared to published eastern equatorial Pacific core top data from cores TR163-11, TR163-14, and VM28-139 (Osborne et al., 2017).

5. Discussion

5.1. The Influence of the Panama Basin Geochemical Environment on Foraminiferal Cadmium

The strong correlation between the bulk planktonic Mn and elements associated with Mn-oxides in middepth core TR163-14 (2.4 km) suggests that precipitation of Mn-oxides is the dominant source of authigenic Mn at this site. This is not surprising as Mn-oxides frequently form on foraminifera and trace element cleaning methods have been developed specifically to address their formation (Boyle & Keigwin, 1985). Furthermore, the presence of Mn-oxides throughout the core indicates that middepth waters remained oxygenated during deglaciation. However, the strong correlation between bulk planktonic Mn and Ce/Ce* suggests that changes in redox potential at this core depth may have begun to overprint the cerium anomaly. Higher glacial Ce/Ce* values indicate that middepth oxygenation was likely reduced during the LGM, although precipitation of Mn-oxides suggests that suboxic conditions were not reached (Yang et al., 1995). This is supported by elevated U/Ca measured in the authigenic coatings of foraminifera from similar water-depth core TR163-25 (2,650 m; Umling & Thunell, 2018), showing that waters at 2.65 km depth had significantly lower oxygen concentrations during the LGM relative to the Holocene. The agreement between the Ce/Ce* and uranium estimates of oxygenation suggests that changes in oxygenation rather than enhanced flux of Ce/Ce*-depleted hydrothermal fluids drove the changes in cerium anomaly documented for TR163-14. Furthermore, the strong correlation between bulk planktonic Cd and Mn indicates that much of the authigenic Cd was incorporated in the Mn-oxide phase and effective removal of this phase should limit contamination of cleaned benthic foraminiferal Cd/Ca values. Low Mn/Ca values of $<$100 μmol/mol have been shown to contribute negligibly to foraminiferal trace element concentrations (Boyle, 1983). The low Mn/Ca values ($<$100 μmol/mol) recorded in the cleaned benthic foraminifera from TR163-14 argue that this phase was indeed effectively removed during cleaning and that we can be confident in the measured benthic Cd/Ca values from this core.

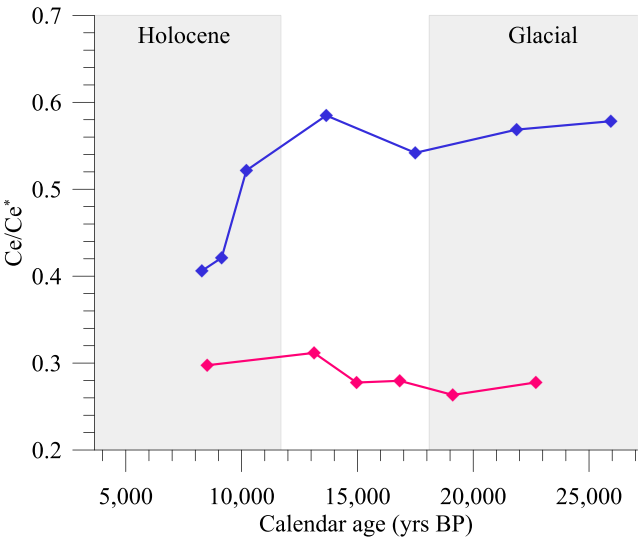

Figure 7. The estimated cerium anomalies (Ce/Ce^*) for middepth (TR163-14; 2.37 km; blue) and deep waters (TR163-20B; 3.20 km; red) over the last glacial-interglacial transition. An abrupt shift in the middepth Ce/Ce^* value at ~13 ka coincides with increasing middepth oxygenation based on uranium from foraminifera authigenic coatings (Umling & Thunell, 2018).

In contrast to the cleaned benthic foraminifera trace element concentrations, bulk planktonic foraminiferal samples from deepwater core TR163-20B (3.2 km) are marked by strong correlations between Mn and the trace elements Cr and Li (Table 2). This differs from the strong correlations recorded for TR163-14 (2.36 km) bulk planktonic foraminifera between Mn and the cerium anomaly, along with Mn and the trace elements Co and Ni. The different trace element associations recorded for TR163-20B bulk planktonic Mn suggest that the authigenic Mn from this core is not influenced by the same processes affecting TR163-14, indicating a reduced influence of authigenic Mn-oxide formation at the deeper core depth. However, both cleaned benthic Mn/Ca and bulk planktonic authigenic Mn were significantly elevated in TR163-20B. In the Panama Basin, hydrothermal plumes associated with the Galapagos spreading center account for a significant source of Mn below ~2 km water depth (Klinkhammer, 1980). TR163-20B shows strong correlations between Li and Mn ($r^2 = 0.97$); hydrothermal activity has been proposed as an important source of Li (Hodkinson et al., 1994) with high concentrations of Li found in hydrothermal-Mn crusts (Glasby et al., 1997). Thus, the close link between bulk planktonic Mn and Li in TR163-20B could indicate a hydrothermal-Mn contribution. However, riverine input and alteration of basalts are also important sources and sinks of Li to sediments (Elderfield & Schultz, 1996) and high

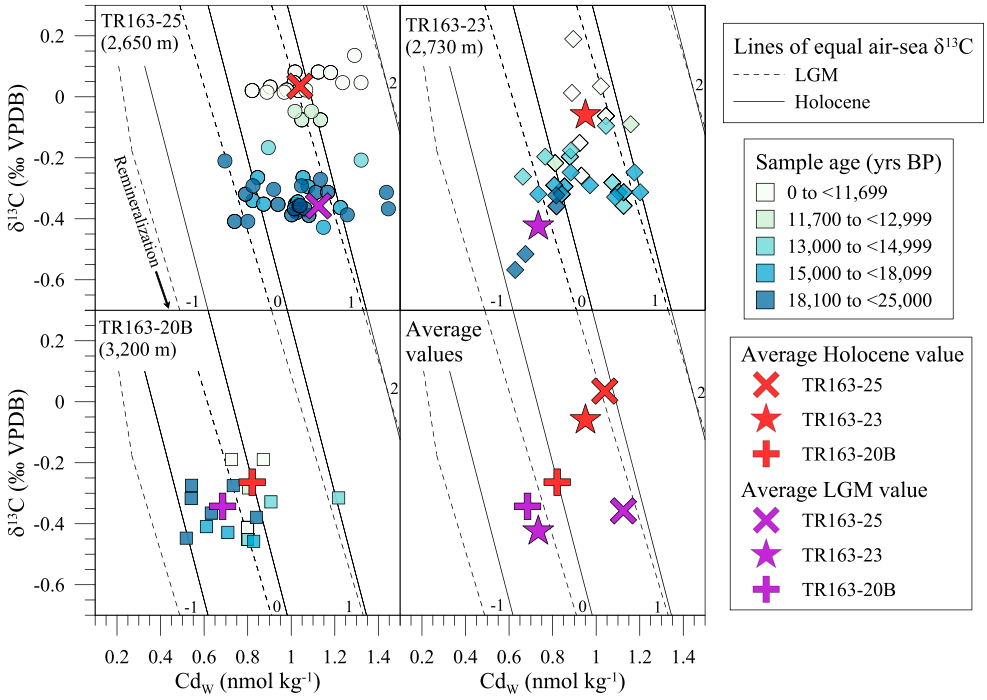

Figure 8. Benthic foraminiferal Cd_W values versus $\delta^{13}C$ for three TR163 cores. The lines of equal $\delta^{13}C_{as}$ are plotted following Lynch-Stieglitz et al. (1995, 1996), accounting for the change in Cd-P slope at P = 1.3 μmol/kg (Boyle, 1988) following Oppo and Horowitz (2000).

concentrations of Li do not unequivocally confirm a hydrothermal source. Variable enrichments of Cd have been recorded in hydrothermal fluids (Von Damm, 1990), raising the possibility of a hydrothermal influence on the Cd/Ca values recorded by TR163-20B. However, the Cd_W values reconstructed from TR163-20B agree well with Cd_W from EEP cores located distally from the Galapagos spreading center (Figure 9; Boyle, 1992) suggesting that a hydrothermal source of Cd was not important.

The flux of hydrothermal-Mn to the sediments and Mn-oxide reduction within the sediments contribute to shallow sedimentary enrichments of Mn(II), which is rapidly removed by mixed Mn-Ca carbonate phases (Pedersen & Price, 1982). The tendency of mixed Mn-Ca carbonate phases to form overgrowths on foraminiferal shells has been documented in the Panama Basin (Boyle, 1983; Pena et al., 2005, 2008). These conditions likely contribute to the elevated Mn/Ca recorded in TR163-20B benthic foraminifera even after aggressive cleaning treatments. Despite the inability to decrease TR163-20B benthic foraminiferal Mn/Ca, the low correlation between bulk planktonic authigenic Mn and Cd concentrations (r^2 = 0.5; Table 2) suggests that this cleaning-resistant phase was potentially not an important source of Cd contamination to TR163-20B benthic foraminiferal Cd/Ca values, allowing a larger benthic Mn/Ca contamination threshold of 1000 μmol/mol for this core. Conversely, correlations for TR163-14 between bulk planktonic foraminiferal Mn and trace element indicators for changing redox conditions (Co, Ni, Ce/Ce*) suggest that authigenic Mn was likely in the form of Mn-oxide coatings, which have a larger potential for Cd-contamination if not successfully removed. This required a lower benthic foraminiferal Mn/Ca contamination threshold of 100 μmol/mol for TR163-14.

5.2. Glacial-Interglacial Deepwater Changes and Carbon Remineralization

Average LGM Cd_W values at 2.0–2.6 km water depth in the EEP were ~0.06 to 0.09 nmol/kg greater than average Holocene values (Figure 5), whereas water depths above and below this layer recorded LGM Cd_W values ~0.13 to 0.22 lower than their Holocene averages. Recent water column measurements of [Cd] and $\delta^{114}Cd$ paired with phosphate concentrations suggest decoupling of Cd and phosphate in low oxygen regions as a result of Cd-sulfide (CdS) precipitation (Janssen et al., 2014). Similarly, the REE and trace element results from TR163-14 suggest that oxygen concentrations at 2.37 km water depth were reduced during the LGM (Figure 7). Increased CdS precipitation under reduced oxygen concentrations could account for the

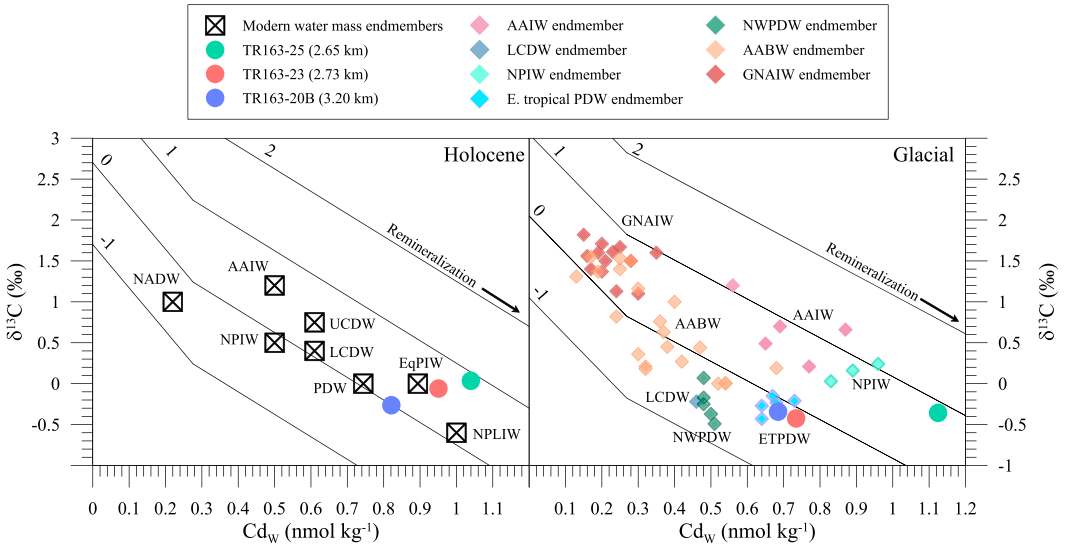

Figure 9. Holocene and glacial Cd_w verses $\delta^{13}C$ values for the water mass end members and the average glacial and Holocene values for the TR163 cores included in Figure 7. Holocene water mass end-members are from the preindustrial $\delta^{13}C$ estimates of Eide et al. (2017) and Cd_w estimates from GLODAPv2 PO_4 (Olsen et al., 2016). Data comprising the Glacial North Atlantic Intermediate Water (GNAIW) end-member include data from intermediate water-depths (400–2000 m) in the North Atlantic (Bertram et al., 1995; Boyle, 1992; Marchitto et al., 1998, 2002; Marchitto & Broecker, 2006; Rickaby et al., 2000; Rickaby & Elderfield, 2005; Willamowski & Zahn, 2000). North Atlantic data from water depths >2 km comprises the Antarctic Bottom Water (AABW) end-member (Bertram et al., 1995; Beveridge et al., 1995; Boyle, 1992; Boyle & Keigwin, 1987; Came et al., 2003; Marchitto et al., 1998, 2002; Willamowski & Zahn, 2000). The LCDW and AAIW end-members include data from the SW Pacific (Lynch-Stieglitz et al., 1996). End-members for Northwest Pacific Deep Water (NWPDW), Eastern Tropical Pacific Deep Water (ETPDW), and North Pacific Intermediate Water (NPIW) are from Boyle (1992). The lines of equal $\delta^{13}C_{as}$ are plotted following Lynch-Stieglitz et al. (1995, 1996), accounting for the change in Cd-P slope at P = 1.3 μmol/kg (Boyle, 1988) following Oppo and Horowitz (2000).

increased glacial Cd_W values and enhanced variability recorded at water depths of ~2.0–2.5 km. However, our REE and trace element results indicate that these waters did not become suboxic ($[O_2]$ = 2 to 10 μmol/kg; Bianchi et al., 2012), and oxygen concentrations may not have been sufficiently low for the formation of Cd-sulfides.

Alternatively, a middepth Cd_W maximum during the LGM could reflect increased phosphate concentrations as predicted by the "nutrient deepening" hypothesis, which suggests a transfer of nutrients and CO_2 from intermediate and middepth waters to deep, abyssal waters under a more efficient biological pump (Boyle, 1988; Jaccard et al., 2009). Middepth cores TR163-23 and TR163-25 both record a shift in $\delta^{13}C$ and Cd_W consistent with a decline in remineralization from the LGM to the Holocene (Figure 8). This suggests that respired carbon accumulated in EEP middepth waters (1.0–3.0 km). A link between biological pump efficiency and ventilation (Sarmiento & Toggweiler, 1984) has been suggested to account for more than half of the recorded atmospheric CO_2 increase during the last deglaciation (Skinner et al., 2017). Furthermore, the deglacial reduction in remineralization coincides with records of increasing middepth ventilation at this time (Burke et al., 2015; Cook & Keigwin, 2015; de la Fuente et al., 2015; Ronge et al., 2016; Sikes et al., 2000, 2016; Skinner et al., 2015, 2017; Umling & Thunell, 2017). Similar Cd_W enrichments and increased variability have also been documented for AAIW at ~1.0–1.5 km water depth in the Sub-Antarctic Pacific (Lynch-Stieglitz et al., 1996). During the formation of AAIW in the Southern Ocean, the high-Cd_w deepwater signature likely becomes entrained in intermediate waters, which are then propagated northward to low latitudes. This link between AAIW and low-latitude surface waters has been previously observed (Anderson et al., 2009; Bova et al., 2015; Spero & Lea, 2002). Similarly, AAIW was marked by reduced ventilation during the LGM (Burke & Robinson, 2012; Sikes et al., 2000, 2016; Skinner et al., 2015) and may have contributed to the radiocarbon depletions documented for shallow waters in the EEP (Umling & Thunell, 2017).

A shift in the source areas and mixing of the deep and middepth water masses in this region could also contribute to changes in remineralization and ventilation. The combined $\delta^{13}C$ and Cd_W results from 2.65 to

3.2 km water depth are useful for distinguishing between changes in water mass mixing and nutrient content (Figure 8). Changes in the proportion of intermediate and deep water masses in mid and deep water depths of the EEP are reflected by changes in the $\delta^{13}C_{as}$ values of these cores. In addition, changes in end-member $\delta^{13}C$ as a result of glacial-interglacial SST variations at the site of deepwater formation will influence end-member $\delta^{13}C_{as}$ values and subsequently, the $\delta^{13}C_{as}$ values recorded at locations influenced by these waters (Broecker & Peng, 1982; Charles et al., 1993; Lynch-Stieglitz et al., 1995). Placing Cd_W-$\delta^{13}C$ results from the EEP in relation to Holocene and glacial end-member values is used to distinguish glacial-interglacial changes in end-member value from changes in water-mass mixing and circulation (Figure 9).

The Holocene water mass composition of deepwater core TR163-20B is a mixture of aged PDW and NPIW (Eide et al., 2017; Olsen et al., 2016; Figure 9). Unfortunately, sediments from the late Holocene were not recovered by sediment core TR163-20B. The Holocene Cd_W-$\delta^{13}C$ results of this core are constrained solely by early-Holocene data (Figure 8). The Cd_W-$\delta^{13}C$ composition of deep waters recorded by TR163-20B indicates a slight increase in average $\delta^{13}C_{as}$ from the LGM to the early-Holocene (Figure 8). Furthermore, a shift in deepwater end-member Cd_W-$\delta^{13}C$ values suggests that the composition of glacial deep EEP waters reflects a different mixture of deepwater masses than bathed the site during the Holocene (Figure 9). The average glacial water-mass composition of TR163-20B is in agreement with previous estimates of Eastern Tropical Pacific Deep Water from Boyle (1992) and reflects a mixture of aged Lower Circumpolar Deep Waters, Northwest Pacific Deep Water, and Antarctic Bottom Water (Boyle, 1992; Lynch-Stieglitz et al., 1996; Figure 9). During the Holocene, middepth core TR163-23 is composed of EqPIW (Eide et al., 2017; Olsen et al., 2016), which is formed by mixing of oxygen-minimum waters of North Pacific Lower Intermediate Water (Eide et al., 2017) with AAIW and upwelled PDW (Bostock et al., 2010). However, middepth core TR163-25 records elevated Cd_w values (>1 nmol/kg) suggesting an influence of high PO_4 (>3 μmol/kg) waters from adjacent oxygen minimum zones (Bostock et al., 2010; Olsen et al., 2016). The elevated Cd_w values may also be influenced by an increased contribution of high-nutrient NPIW to EqPIW during the LGM, at the expense of AAIW (Rippert et al., 2017).

The average EEP Holocene $\delta^{13}C_{as}$ values show a progression from the low $\delta^{13}C_{as}$ values of TR163-20B (−0.07‰) to the higher values of TR163-23 (0.58‰) and TR163-25 (0.96‰). However, these cores document a different vertical distribution of average $\delta^{13}C_{as}$ values during the LGM, with a decreased LGM $\delta^{13}C_{as}$ difference between TR163-23 and TR163-20B of 0.14‰ relative to 0.64‰ during the Holocene (Figure 8). Conversely, the offset between TR163-25 and TR163-23 increased from 0.39‰ during the Holocene to 1.01‰ during the LGM (Figure 8). The shift in the vertical distribution of average $\delta^{13}C_{as}$ values is primarily driven by a 0.732‰ decrease in the average TR163-23 LGM $\delta^{13}C_{as}$ value relative to the Holocene (Figure 8). Cores TR163-25 and TR163-20B document smaller LGM-Holocene offsets of 0.11‰ and −0.23, respectively (Figure 8). The similarity in LGM $\delta^{13}C_{as}$ values recorded by TR163-23 and TR163-20B suggests an increased influence of deeper water masses with lower $\delta^{13}C_{as}$ values at 2.73 km water depth at this time, whereas end-member Cd_W-$\delta^{13}C$ values suggest that waters at site TR163-25 were primarily influenced by aged NPIW and AAIW during the LGM (Figure 9). However, additional carbon isotopic records from the southwest and southeast Pacific suggest that the $\delta^{13}C$ value of Circumpolar Deep Water (CDW) was as low as −0.5‰ to −0.8‰ during the LGM (McCave et al., 2008; Sikes et al., 2016; Ullermann et al., 2016). Although benthic foraminiferal Cd/Ca is not available for these cores, records of carbonate chemistry from benthic foraminifera B/Ca suggest that the low glacial $\delta^{13}C$ values documented for the southwest Pacific are likely driven by increased respired carbon storage (Allen et al., 2015). Furthermore, similar changes in carbonate chemistry have been recorded in the equatorial Pacific (Umling & Thunell, 2018; Yu et al., 2013) consistent with a contribution of CDW to equatorial Pacific mid and deep water depths.

These results suggest that enhanced vertical mixing of CDW may contribute to the lower glacial $\delta^{13}C$ values recorded by TR163-23. Although CDW in the EEP likely mixed to water depths as shallow as 2.73 km, it was probably not an important contribution to waters at 2.65 km water depth. This finding provides further support for a shoaling of the isopycnal separating the upper and lower branches of SOOC (Burke et al., 2015), which has been suggested as a mechanism for respired carbon accumulation and reduced ventilation in middepth waters (Ferrari et al., 2014). Furthermore, the findings of enhanced EEP middepth remineralization support radiocarbon records of ventilation, which suggest reduced ventilation during the LGM (de la Fuente

et al., 2015; Umling & Thunell, 2017). It has been hypothesized that increased input of ^{14}C-depleted mantle carbon could be responsible for reduced foraminiferal ^{14}C values recorded at middepths during the LGM (Hasenclever et al., 2017; Lund et al., 2016). The findings of enhanced remineralization in this study suggest that reduced ventilation, rather than increased influence of mantle carbon, was probably the primary influence on the ^{14}C-ventilation records from this region (de la Fuente et al., 2015; Umling & Thunell, 2017). However, a combined influence of both reduced ventilation and an increased flux of carbon from the mantle cannot be ruled out without records of past carbon flux from the mantle.

6. Conclusions

The Panama Basin has a complex geochemical environment due to venting of hydrothermal fluids to deep waters (Klinkhammer et al., 1977; Marchig et al., 1984), subaerial and submarine volcanism (Kowsmann, 1973; Lea et al., 2005), varying water column redox conditions, and high surface productivity (Pennington et al., 2006). Each of these processes can impact foraminiferal trace element chemistry to varying extents, but their impact is spatially variable throughout the basin. Formation of manganese-oxides has the potential for increasing the foraminiferal Cd/Ca values, but Mn/Ca values <100 μmol/mol have been shown to indicate negligible elevation of Cd/Ca suggesting successful removal of Mn-oxide contamination (Boyle, 1983; Boyle & Keigwin, 1985). Our authigenic trace element results from bulk planktonic foraminifera suggest that Mn coatings are unlikely to be a significant contributor to the Cd/Ca values of the cleaned benthic foraminifera samples from TR163-20B.

Our paired Cd/Ca and $\delta^{13}C$ records are consistent with respired carbon accumulation in middepth waters along with increased influence of deepwater masses at ~2.7 km water-depth during the LGM. Taken together, the Cd_W-$\delta^{13}C$ results of remineralization and mixing suggest both an expansion of deepwater masses to water depths of ~2.7 km along with increased remineralization at midwater depths. These results support the findings of ^{14}C-derived records of ventilation, which indicate a reduction of EEP middepth ventilation during the LGM (de la Fuente et al., 2015; Umling & Thunell, 2017). Furthermore, this combination of findings provides some support for the conceptual premise that a shoaling of the isopycnal separating the upper and lower branches of SOOC under increased Antarctic sea ice extent would have allowed respired carbon to accumulate and radiocarbon to decay in middepth waters (Burke et al., 2015; Ferrari et al., 2014).

Acknowledgments
We thank E. Tappa, B. Bair, W. Buckley, and C. Chartier for laboratory assistance. We thank S. Carey from the University of Rhode Island Core Repository for providing the samples used in this study. Support for this curating facility is provided by the National Science foundation through grant OCE-0956368. The authors declare no competing financial interests. The data supporting the conclusions can be found in the supporting information.

References

Allen, K. A., Sikes, E. L., Hönisch, B., Elmore, A. C., Guilderson, T. P., Rosenthal, Y., & Anderson, R. F. (2015). Southwest Pacific deep water carbonate chemistry linked to high southern latitude climate and atmospheric CO_2 during the last glacial termination. *Quaternary Science Reviews*, *122*, 180–191. https://doi.org/10.1016/j.quascirev.2015.05.007

Anderson, R. F., Ali, S., Bradtmiller, L. I., Nielsen, S. H. H., Fleisher, M. Q., Anderson, B. E., & Burckle, L. H. (2009). Wind-driven upwelling in the Southern Ocean and the Deglacial rise in atmospheric CO_2. *Science*, *323*(5920), 1443–1448. https://doi.org/10.1126/science.1167441

Balistrieri, L. S., & Murray, J. W. (1986). The surface chemistry of sediments from the Panama Basin: The influence of Mn oxides on metal adsorption. *Geochimica et Cosmochimica Acta*, *50*(10), 2235–2243. https://doi.org/10.1016/0016-7037(86)90078-5

Barker, S., Greaves, M., & Elderfield, H. (2003). A study of cleaning procedures used for foraminiferal Mg/Ca paleothermometry. *Geochemistry, Geophysics, Geosystems*, *4*(9), 8407. https://doi.org/10.1029/2003GC000559

Bauska, T. K., Baggenstos, D., Brook, E. J., Mix, A. C., Marcott, S. A., Petrenko, V. V., et al. (2016). Carbon isotopes characterize rapid changes in atmospheric carbon dioxide during the last deglaciation. *Proceedings of the National Academy of Sciences of the United States of America*, *113*(13), 3465–3470. https://doi.org/10.1073/pnas.1513868113

Bertram, C. J., Elderfield, H., Shackleton, N. J., & MacDonald, J. A. (1995). Cadmium/calcium and carbon isotope reconstructions of the glacial northeast Atlantic Ocean. *Paleoceanography*, *10*(3), 563–578. https://doi.org/10.1029/94PA03058

Beveridge, N. A. S., Elderfield, H., & Shackleton, N. J. (1995). Deep thermohaline circulation in the low-latitude Atlantic during the last glacial. *Paleoceanography*, *10*(3), 643–660. https://doi.org/10.1029/94PA03353

Bianchi, D., Dunne, J. P., Sarmiento, J. L., & Galbraith, E. D. (2012). Data-based estimates of suboxia, denitrification, and N_2O production in the ocean and their sensitivities to dissolved O_2. *Global Biogeochemical Cycles*, *26*, GB2009. https://doi.org/10.1029/2011GB004209

Blaauw, M., & Christen, J. A. (2011). Flexible paleoclimate age-depth models using an autoregressive gamma process. *Bayesian Analysis*, *6*(3), 457–474. https://doi.org/10.1214/11-BA618

Bostock, H. C., Opdyke, B. N., & Williams, M. J. M. (2010). Characterizing the intermediate depth waters of the Pacific Ocean using $\delta^{13}C$ and other geochemical tracers. *Deep Sea Research Part I: Oceanographic Research Papers*, *57*(7), 847–859. https://doi.org/10.1016/j.dsr.2010.04.005

Bova, S. C., Herbert, T., Rosenthal, Y., Kalansky, J., Altabet, M., Chazen, C., et al. (2015). Links between eastern equatorial Pacific stratification and atmospheric CO_2 rise during the last deglaciation. *Paleoceanography*, *30*, 1407–1424. https://doi.org/10.1002/2015PA002816

Boyle, E. A. (1981). Cadmium, zinc, copper, and barium in foraminifera tests. *Earth and Planetary Science Letters*, *53*(1), 11–35. https://doi.org/10.1016/0012-821X(81)90022-4

Boyle, E. A. (1983). Manganese carbonate overgrowths on foraminifera tests. *Geochimica et Cosmochimica Acta*, *47*(10), 1815–1819. https://doi.org/10.1016/0016-7037(83)90029-7

Boyle, E. A. (1988). Cadmium: Chemical tracer of deep water paleoceanography. *Paleoceanography*, *3*(4), 471–489. https://doi.org/10.1029/PA003i004p00471

Boyle, E. A. (1992). Cadmium and delta13C paleochemical ocean distributions during the stage 2 glacial maximum. *Annual Review of Earth and Planetary Sciences*, *20*(1), 245–287. https://doi.org/10.1146/annurev.ea.20.050192.001333

Boyle, E. A., & Keigwin, L. (1987). North Atlantic thermohaline circulation during the past 20,000 years linked to high-latitude surface temperature. *Nature*, *330*(6143), 35–40. https://doi.org/10.1038/330035a0

Boyle, E. A., & Keigwin, L. D. (1985). Comparison of Atlantic and Pacific paleochemical records for the last 215,000 years: Changes in deep ocean circulation and chemical inventories. *Earth and Planetary Science Letters*, *76*(1–2), 135–150. https://doi.org/10.1016/0012-821X(85)90154-2

Boyle, E. A., & Rosenthal, Y. (1996). Chemical hydrography of the South Atlantic during the last glacial maximum: Cd vs. d13C. In *The South Atlantic: Present and Past Circulation* (pp. 423–443). Verlag: Springer.

Broecker, W., & Barker, S. (2007). A 190‰ drop in atmosphere's $\Delta^{14}C$ during the "Mystery Interval" (17.5 to 14.5 kyr). *Earth and Planetary Science Letters*, *256*(1–2), 90–99. https://doi.org/10.1016/j.epsl.2007.01.015

Broecker, W. S. (1982). Glacial to interglacial changes in ocean chemistry. *Progress in Oceanography*, *11*(2), 151–197. https://doi.org/10.1016/0079-6611(82)90007-6

Broecker, W. S., & Peng, T.-H. (1982). Tracers in the Sea. Lamont-Doherty Geological Observatory, Columbia University.

Burke, A., & Robinson, L. F. (2012). The Southern Ocean's role in carbon exchange during the last deglaciation. *Science*, *335*(6068), 557–561. https://doi.org/10.1126/science.1208163

Burke, A., Stewart, A. L., Adkins, J. F., Ferrari, R., Jansen, M. F., & Thompson, A. F. (2015). The glacial mid-depth radiocarbon bulge and its implications for the overturning circulation. *Paleoceanography*, *30*, 1021–1039. https://doi.org/10.1002/2015PA002778

Came, R. E., Oppo, D. W., & Curry, W. B. (2003). Atlantic Ocean circulation during the younger Dryas: Insights from a new Cd/Ca record from the western subtropical South Atlantic. *Paleoceanography*, *18*(4), 1086. https://doi.org/10.1029/2003PA000888

Charles, C. D., Wright, J. D., & Fairbanks, R. G. (1993). Thermodynamic influences on the marine carbon isotope record. *Paleoceanography*, *8*(6), 691–697. https://doi.org/10.1029/93PA01803

Cook, M. S., & Keigwin, L. D. (2015). Radiocarbon profiles of the NW Pacific from the LGM and deglaciation: Evaluating ventilation metrics and the effect of uncertain surface reservoir ages: Northwest Pacific radiocarbon. *Paleoceanography*, *30*, 174–195. https://doi.org/10.1002/2014PA002649

Curry, W. B., Duplessy, J. C., Labeyrie, L. D., & Shackleton, N. J. (1988). Changes in the distribution of $\delta^{13}C$ of deep water ΣCO_2 between the last glaciation and the Holocene. *Paleoceanography*, *3*(3), 317–341. https://doi.org/10.1029/PA003i003p00317

de la Fuente, M., Skinner, L., Calvo, E., Pelejero, C., & Cacho, I. (2015). Increased reservoir ages and poorly ventilated deep waters inferred in the glacial eastern equatorial Pacific. *Nature Communications*, *6*(1), 7420. https://doi.org/10.1038/ncomms8420

Eide, M., Olsen, A., Ninnemann, U. S., & Johannessen, T. (2017). A global ocean climatology of preindustrial and modern ocean $\delta^{13}C$: Climatology of preindustrial $\delta^{13}C$. *Global Biogeochemical Cycles*, *31*, 515–534. https://doi.org/10.1002/2016GB005473

Elderfield, H., & Greaves, M. J. (1982). The rare earth elements in seawater. *Nature*, *296*(5854), 214–219. https://doi.org/10.1038/296214a0

Elderfield, H., & Schultz, A. (1996). Mid-Ocean ridge hydrothermal fluxes and the chemical composition of the ocean. *Annual Review of Earth and Planetary Sciences*, *24*(1), 191–224. https://doi.org/10.1146/annurev.earth.24.1.191

Ferrari, R., Jansen, M. F., Adkins, J. F., Burke, A., Stewart, A. L., & Thompson, A. F. (2014). Antarctic Sea ice control on ocean circulation in present and glacial climates. *Proceedings of the National Academy of Sciences of the United States of America*, *111*(24), 8753–8758. https://doi.org/10.1073/pnas.1323922111

Fiedler, P. C., & Talley, L. D. (2006). Hydrography of the eastern tropical Pacific: A review. *Progress in Oceanography*, *69*(2–4), 143–180. https://doi.org/10.1016/j.pocean.2006.03.008

Galbraith, E. D., & Eggleston, S. (2017). A lower limit to atmospheric CO_2 concentrations over the past 800,000 years. *Nature Geoscience*, *10*(4), 295–298. https://doi.org/10.1038/ngeo2914

German, C. R., & Elderfield, H. (1990). Application of the Ce anomaly as a paleoredox indicator: The ground rules. *Paleoceanography*, *5*(5), 823–833. https://doi.org/10.1029/PA005i005p00823

Glasby, G. P., Stüben, D., Jeschke, G., Stoffers, P., & Garbe-Schönberg, C.-D. (1997). A model for the formation of hydrothermal manganese crusts from the Pitcairn Island hotspot. *Geochimica et Cosmochimica Acta*, *61*(21), 4583–4597. https://doi.org/10.1016/S0016-7037(97)00262-7

Hasenclever, J., Knorr, G., Rüpke, L. H., Köhler, P., Morgan, J., Garofalo, K., et al. (2017). Sea level fall during glaciation stabilized atmospheric CO_2 by enhanced volcanic degassing. *Nature Communications*, *8*, 15,867. https://doi.org/10.1038/ncomms15867

Heaton, T. J., Bard, E., & Hughen, K. A. (2013). Elastic tie-pointing—Transferring chronologies between records via a Gaussian process. *Radiocarbon*, *55*(04), 1975–1997. https://doi.org/10.2458/azu_js_rc.55.17777

Hertzberg, J. E., Lund, D. C., Schmittner, A., & Skrivanek, A. L. (2016). Evidence for a biological pump driver of atmospheric CO_2 rise during Heinrich Stadial 1. *Geophysical Research Letters*, *43*, 12,242–12,251. https://doi.org/10.1002/2016GL070723

Hodkinson, R. A., Stoffers, P., Scholten, J., Cronan, D. S., Jeschke, G., & Rogers, T. D. S. (1994). Geochemistry of hydrothermal manganese deposits from the Pitcairn Island hotspot, southeastern Pacific. *Geochimica et Cosmochimica Acta*, *58*(22), 5011–5029. https://doi.org/10.1016/0016-7037(94)90228-3

Hughen, K. (2004). ^{14}C activity and global carbon cycle changes over the past 50,000 years. *Science*, *303*(5655), 202–207. https://doi.org/10.1126/science.1090300

Hughen, K. A., Overpeck, J. T., Lehman, S. J., Kashgarian, M., Southon, J., Peterson, L. C., et al. (1998). Deglacial changes in ocean circulation from an extended radiocarbon calibration. *Nature*, *391*(6662), 65–68. https://doi.org/10.1038/34150

Hughen, K. A., Southon, J. R., Lehman, S. J., & Overpeck, J. T. (2000). Synchronous radiocarbon and climate shifts during the last deglaciation. *Science*, *290*(5498), 1951–1955.

Inoue, H., & Sugimura, Y. (1985). Carbon isotopic fractionation during the CO_2 exchange process between air and sea water under equilibrium and kinetic conditions. *Geochimica et Cosmochimica Acta*, *49*(11), 2453–2460. https://doi.org/10.1016/0016-7037(85)90245-5

Jaccard, S. L., Galbraith, E. D., Martínez-García, A., & Anderson, R. F. (2016). Covariation of deep Southern Ocean oxygenation and atmospheric CO_2 through the last ice age. *Nature*, *530*(7589), 207–210. https://doi.org/10.1038/nature16514

Jaccard, S. L., Galbraith, E. D., Sigman, D. M., Haug, G. H., Francois, R., Pedersen, T. F., et al. (2009). Subarctic Pacific evidence for a glacial deepening of the oceanic respired carbon pool. *Earth and Planetary Science Letters*, *277*(1–2), 156–165. https://doi.org/10.1016/j.epsl.2008.10.017

Janssen, D. J., Conway, T. M., John, S. G., Christian, J. R., Kramer, D. I., Pedersen, T. F., & Cullen, J. T. (2014). Undocumented water column sink for cadmium in open ocean oxygen-deficient zones. *Proceedings of the National Academy of Sciences of the United States of America*, *111*(19), 6888–6893. https://doi.org/10.1073/pnas.1402388111

Kamykowski, D., & Zentara, S.-J. (1990). Hypoxia in the world ocean as recorded in the historical data set. *Deep Sea Research Part A. Oceanographic Research Papers*, *37*(12), 1861–1874. https://doi.org/10.1016/0198-0149(90)90082-7

Keeling, R. F., & Stephens, B. B. (2001). Antarctic sea ice and the control of Pleistocene climate instability. *Paleoceanography*, *16*(1), 112–131. https://doi.org/10.1029/2000PA000529

Key, R. M., Kozyr, A., Sabine, C. L., Lee, K., Wanninkhof, R., Bullister, J. L., et al. (2004). A global ocean carbon climatology: Results from Global Data Analysis Project (GLODAP). *Global Biogeochemical Cycles*, *18*, GB4031. https://doi.org/10.1029/2004GB002247

Klinkhammer, G., Bender, M., & Weiss, R. F. (1977). Hydrothermal manganese in the Galapagos Rift. *Nature*, *269*(5626), 319–320. https://doi.org/10.1038/269319a0

Klinkhammer, G. P. (1980). Observations of the distribution of manganese over the East Pacific Rise. *Chemical Geology*, *29*(1–4), 211–226. https://doi.org/10.1016/0009-2541(80)90021-2

Kohfeld, K. E. (2005). Role of marine biology in glacial-interglacial CO_2 cycles. *Science*, *308*(5718), 74–78. https://doi.org/10.1126/science.1105375

Kowsmann, R. O. (1973). Coarse components in surface sediments of the Panama Basin, eastern equatorial Pacific. *The Journal of Geology*, *81*(4), 473–494. https://doi.org/10.1086/627885

Lea, D. W., Pak, D. K., & Paradis, G. (2005). Influence of volcanic shards on foraminiferal Mg/Ca in a core from the Galápagos region. *Geochemistry, Geophysics, Geosystems*, *6*, Q11P04. https://doi.org/10.1029/2005GC000970

Lonsdale, P. (1976). Abyssal circulation of the southeastern Pacific and some geological implications. *Journal of Geophysical Research*, *81*(6), 1163–1176. https://doi.org/10.1029/JC081i006p01163

Lund, D. C. (2013). Deep Pacific ventilation ages during the last deglaciation: Evaluating the influence of diffusive mixing and source region reservoir age. *Earth and Planetary Science Letters*, *381*, 52–62. https://doi.org/10.1016/j.epsl.2013.08.032

Lund, D. C., Asimow, P. D., Farley, K. A., Rooney, T. O., Seeley, E., Jackson, E. W., & Durham, Z. M. (2016). Enhanced East Pacific Rise hydrothermal activity during the last two glacial terminations. *Science*, *351*(6272), 478–482. https://doi.org/10.1126/science.aad4296

Lynch-Stieglitz, J., & Fairbanks, R. G. (1994). A conservative tracer for glacial ocean circulation from carbon isotope and palaeo-nutrient measurements in benthic foraminifera. *Nature*, *369*(6478), 308–310. https://doi.org/10.1038/369308a0

Lynch-Stieglitz, J., Stocker, T. F., Broecker, W. S., & Fairbanks, R. G. (1995). The influence of air-sea exchange on the isotopic composition of oceanic carbon: Observations and modeling. *Global Biogeochemical Cycles*, *9*(4), 653–665. https://doi.org/10.1029/95GB02574

Lynch-Stieglitz, J., van Geen, A., & Fairbanks, R. G. (1996). Interocean exchange of glacial North Atlantic Intermediate Water: Evidence from subantarctic Cd/Ca and carbon isotope measurements. *Paleoceanography*, *11*(2), 191–201. https://doi.org/10.1029/95PA03772

Mackensen, A. (2008). On the use of benthic foraminiferal $\delta^{13}C$ in palaeoceanography: Constraints from primary proxy relationships. *Geological Society, London, Special Publications*, *303*(1), 121–133. https://doi.org/10.1144/SP303.9

Marchig, V., Möller, P., Bäcker, H., & Dulski, P. (1984). Foraminiferal ooze from the Galapagos Rift area-hydrothermal impact and diagenetic mobilization of elements. *Marine Geology*, *62*(1–2), 85–104. https://doi.org/10.1016/0025-3227(84)90056-2

Marchitto, T. M., & Broecker, W. S. (2006). Deep water mass geometry in the glacial Atlantic Ocean: A review of constraints from the paleo-nutrient proxy Cd/Ca. *Geochemistry, Geophysics, Geosystems*, *7*, Q12003. https://doi.org/10.1029/2006GC001323

Marchitto, T. M., Curry, W. B., & Oppo, D. W. (1998). Millennial-scale changes in North Atlantic circulation since the last glaciation. *Nature*, *393*(6685), 557–561. https://doi.org/10.1038/31197

Marchitto, T. M., Oppo, D. W., & Curry, W. B. (2002). Paired benthic foraminiferal cd/ca and Zn/ca evidence for a greatly increased presence of Southern Ocean water in the glacial North Atlantic. *Paleoceanography*, *17*(3), 1038. https://doi.org/10.1029/2000PA000598

Marcott, S. A., Bauska, T. K., Buizert, C., Steig, E. J., Rosen, J. L., Cuffey, K. M., et al. (2014). Centennial-scale changes in the global carbon cycle during the last deglaciation. *Nature*, *514*(7524), 616–619. https://doi.org/10.1038/nature13799

McCave, I. N., Carter, L., & Hall, I. R. (2008). Glacial–interglacial changes in water mass structure and flow in the SW Pacific Ocean. *Quaternary Science Reviews*, *27*(19–20), 1886–1908. https://doi.org/10.1016/j.quascirev.2008.07.010

Monnin, E., Indermühle, A., Dällenbach, A., Flückiger, J., Stauffer, B., Stocker, T. F., et al. (2001). Atmospheric CO_2 concentrations over the last glacial termination. *Science*, *291*(5501), 112–114. https://doi.org/10.1126/science.291.5501.112

Olsen, A., Key, R. M., van Heuven, S., Lauvset, S. K., Velo, A., Lin, X., et al. (2016). The Global Ocean Data Analysis Project version 2 (GLODAPv2)—An internally consistent data product for the world ocean. *Earth System Science Data*, *8*(2), 297–323. https://doi.org/10.5194/essd-8-297-2016

Oppo, D. W., & Horowitz, M. (2000). Glacial deep water geometry: South Atlantic benthic foraminiferal Cd/Ca and $\delta^{13}C$ evidence. *Paleoceanography*, *15*(2), 147–160. https://doi.org/10.1029%2F1999PA000436

Osborne, A. H., Hathorne, E. C., Schijf, J., Plancherel, Y., Böning, P., & Frank, M. (2017). The potential of sedimentary foraminiferal rare earth element patterns to trace water masses in the past. *Geochemistry, Geophysics, Geosystems*, *18*, 1550–1568. https://doi.org/10.1002/2016GC006782

Pedersen, T. F. (1979). *The geochemistry of sediments of the Panama Basin, eastern equatorial Pacific Ocean*, (PhD dissertation). University of Edinburgh.

Pedersen, T. F., & Price, N. B. (1982). The geochemistry of manganese carbonate in Panama Basin sediments. *Geochimica et Cosmochimica Acta*, *46*(1), 59–68. https://doi.org/10.1016/0016-7037(82)90290-3

Pena, L. D., Cacho, I., Calvo, E., Pelejero, C., Eggins, S., & Sadekov, A. (2008). Characterization of contaminant phases in foraminifera carbonates by electron microprobe mapping. *Geochemistry, Geophysics, Geosystems*, *9*, Q07012. https://doi.org/10.1029/2008GC002018

Pena, L. D., Calvo, E., Cacho, I., Eggins, S., & Pelejero, C. (2005). Identification and removal of Mn-Mg-rich contaminant phases on foraminiferal tests: Implications for Mg/Ca past temperature reconstructions: Mg/Ca. *Geochemistry, Geophysics, Geosystems*, *6*, Q09P02. https://doi.org/10.1029/2005GC000930

Pennington, J. T., Mahoney, K. L., Kuwahara, V. S., Kolber, D. D., Calienes, R., & Chavez, F. P. (2006). Primary production in the eastern tropical Pacific: A review. *Progress in Oceanography*, *69*(2–4), 285–317. https://doi.org/10.1016/j.pocean.2006.03.012

Pichevin, L. E., Reynolds, B. C., Ganeshram, R. S., Cacho, I., Pena, L., Keefe, K., & Ellam, R. M. (2009). Enhanced carbon pump inferred from relaxation of nutrient limitation in the glacial ocean. *Nature*, *459*(7250), 1114–1117. https://doi.org/10.1038/nature08101

Rickaby, R. E. M., & Elderfield, H. (2005). Evidence from the high-latitude North Atlantic for variations in Antarctic Intermediate water flow during the last deglaciation. *Geochemistry, Geophysics, Geosystems*, *6*, Q05001. https://doi.org/10.1029/2004GC000858

Rickaby, R. E. M., Greaves, M. J., & Elderfield, H. (2000). Cd in planktonic and benthic foraminiferal shells determined by thermal ionisation mass spectrometry. *Geochimica et Cosmochimica Acta*, *64*(7), 1229–1236. https://doi.org/10.1016/S0016-7037(99)00317-8

Rippert, N., Max, L., Mackensen, A., Cacho, I., Povea, P., & Tiedemann, R. (2017). Alternating influence of northern versus southern-sourced water masses on the equatorial Pacific subthermocline during the past 240 ka: Water masses of the equatorial Pacific. *Paleoceanography*, *32*, 1256–1274. https://doi.org/10.1002/2017PA003133

Ronge, T. A., Tiedemann, R., Lamy, F., Köhler, P., Alloway, B. V., De Pol-Holz, R., et al. (2016). Radiocarbon constraints on the extent and evolution of the South Pacific glacial carbon pool. *Nature Communications*, *7*, 11487. https://doi.org/10.1038/ncomms11487

Sarmiento, J. L., & Toggweiler, J. R. (1984). A new model for the role of the oceans in determining atmospheric PCO_2. *Nature*, *308*(5960), 621–624. https://doi.org/10.1038/308621a0

Schlitzer, R. (2015). Ocean Data View, odv.awi.de

Schmittner, A., Bostock, H. C., Cartapanis, O., Curry, W. B., Filipsson, H. L., Galbraith, E. D., et al. (2017). Calibration of the carbon isotope composition ($\delta^{13}C$) of benthic foraminifera: Benthic $\delta\ ^{13}C$ calibration. *Paleoceanography*, *32*, 512–530. https://doi.org/10.1002/2016PA003072

Shackleton, N. J., Duplessy, J.-C., Arnold, M., Maurice, P., Hall, M. A., & Cartlidge, J. (1988). Radiocarbon age of last glacial Pacific deep water. *Nature*, *335*(6192), 708–711. https://doi.org/10.1038/335708a0

Sigman, D. M., & Boyle, E. A. (2000). Glacial/interglacial variations in atmospheric carbon dioxide. *Nature*, *407*(6806), 859–869. https://doi.org/10.1038/35038000

Sikes, E. L., Cook, M. S., & Guilderson, T. P. (2016). Reduced deep ocean ventilation in the southern Pacific Ocean during the last glaciation persisted into the deglaciation. *Earth and Planetary Science Letters*, *438*, 130–138. https://doi.org/10.1016/j.epsl.2015.12.039

Sikes, E. L., Elmore, A. C., Allen, K. A., Cook, M. S., & Guilderson, T. P. (2016). Glacial water mass structure and rapid δ18O and δ13C changes during the last glacial termination in the Southwest Pacific. *Earth and Planetary Science Letters*, *456*, 87–97. https://doi.org/10.1016/j.epsl.2016.09.043

Sikes, E. L., Samson, C. R., Guilderson, T. P., & Howard, W. R. (2000). Old radiocarbon ages in the southwest Pacific Ocean during the last glacial period and deglaciation. *Nature*, *405*(6786), 555–559. https://doi.org/10.1038/35014581

Skinner, L., McCave, I. N., Carter, L., Fallon, S., Scrivner, A. E., & Primeau, F. (2015). Reduced ventilation and enhanced magnitude of the deep Pacific carbon pool during the last glacial period. *Earth and Planetary Science Letters*, *411*, 45–52. https://doi.org/10.1016/j.epsl.2014.11.024

Skinner, L. C., Fallon, S., Waelbroeck, C., Michel, E., & Barker, S. (2010). Ventilation of the Deep Southern Ocean and Deglacial CO_2 rise. *Science*, *328*(5982), 1147–1151. https://doi.org/10.1126/science.1183627

Skinner, L. C., Primeau, F., Freeman, E., de la Fuente, M., Goodwin, P. A., Gottschalk, J., et al. (2017). Radiocarbon constraints on the glacial ocean circulation and its impact on atmospheric CO_2. *Nature Communications*, *8*, 16010. https://doi.org/10.1038/ncomms16010

Spero, H. J., & Lea, D. W. (2002). The cause of Carbon Isotope Minimum Events on Glacial Terminations. *Science*, *296*(5567), 522–525. https://doi.org/10.1126%2Fscience.1069401

Taylor, S. R., & McLennan, S. M. (1985). *The continental crust: Its composition and evolution*. Oxford, UK: Blackwell Sci.

Toggweiler, J. R., Russell, J. L., & Carson, S. R. (2006). Midlatitude westerlies, atmospheric CO_2, and climate change during the ice ages. *Paleoceanography*, *21*, PA2005. https://doi.org/10.1029/2005PA001154

Tribovillard, N., Algeo, T. J., Lyons, T., & Riboulleau, A. (2006). Trace metals as paleoredox and paleoproductivity proxies: An update. *Chemical Geology*, *232*(1–2), 12–32. https://doi.org/10.1016/j.chemgeo.2006.02.012

Tsuchiya, M., & Talley, L. D. (1998). A Pacific hydrographic section at 88°W: Water-property distribution. *Journal of Geophysical Research*, *103*(C6), 12,899–12,918. https://doi.org/10.1029/97JC03415

Ullermann, J., Lamy, F., Ninnemann, U., Lembke-Jene, L., Gersonde, R., & Tiedemann, R. (2016). Pacific-Atlantic Circumpolar Deep Water coupling during the last 500 ka. *Paleoceanography*, *31*, 639–650. https://doi.org/10.1002/2016PA002932

Umling, N. E., & Thunell, R. C. (2017). Synchronous deglacial thermocline and deep-water ventilation in the eastern equatorial Pacific. *Nature Communications*, *8*, 14203. https://doi.org/10.1038/ncomms14203

Umling, N. E., & Thunell, R. C. (2018). Mid-depth respired carbon storage and oxygenation of the eastern equatorial Pacific over the last 25,000 years. *Quaternary Science Reviews*, *189*, 43–56. https://doi.org/10.1016/j.quascirev.2018.04.002

Von Damm, K. L. (1990). Seafloor hydrothermal activity: Black smoker chemistry and chimneys. *Annual Review of Earth and Planetary Sciences*, *18*(1), 173–204. https://doi.org/10.1146/annurev.ea.18.050190.001133

Watson, A. J., Vallis, G. K., & Nikurashin, M. (2015). Southern Ocean buoyancy forcing of ocean ventilation and glacial atmospheric CO_2. *Nature Geoscience*, *8*(11), 861–864. https://doi.org/10.1038/ngeo2538

Willamowski, C., & Zahn, R. (2000). Upper ocean circulation in the glacial North Atlantic from benthic foraminiferal isotope and trace element fingerprinting. *Paleoceanography*, *15*(5), 515–527. https://doi.org/10.1029/1999PA000467

Willbold, M., Jochum, K. P., Raczek, I., Amini, M. A., Stoll, B., & Hofmann, A. W. (2003). Validation of multi-element isotope dilution ICPMS for the analysis of basalts. *Analytical and Bioanalytical Chemistry*, *377*(1), 117–125. https://doi.org/10.1007/s00216-003-2037-4

Wright, J., Schrader, H., & Holser, W. T. (1987). Paleoredox variations in ancient oceans recorded by rare earth elements in fossil apatite. *Geochimica et Cosmochimica Acta*, *51*(3), 631–644. https://doi.org/10.1016/0016-7037(87)90075-5

Yang, Y.-L., Elderfield, H., Pedersen, T. F., & Ivanovich, M. (1995). Geochemical record of the Panama basin during the last glacial maximum carbon event shows that the glacial ocean was not suboxic. *Geology*, *23*(12), 1115. https://doi.org/10.1130/0091-7613(1995)023%3C1115:GROTPB%3E2.3.CO;2

Yu, J., Anderson, R. F., Jin, Z., Rae, J. W. B., Opdyke, B. N., & Eggins, S. M. (2013). Responses of the deep ocean carbonate system to carbon reorganization during the Last Glacial-interglacial cycle. *Quaternary Science Reviews*, *76*, 39–52. https://doi.org/10.1016%2Fj.quascirev.2013.06.020

Ziegler, M., Diz, P., Hall, I. R., & Zahn, R. (2013). Millennial-scale changes in atmospheric CO_2 levels linked to the Southern Ocean carbon isotope gradient and dust flux. *Nature Geoscience*, *6*(6), 457–461. https://doi.org/10.1038/ngeo1782